7-2020

Casimir Effect on Amplitude-Frequency Response of Parametric Resonance of Electrostatically Actuated NEMS Cantilever Resonators

Dumitru Caruntu
The University of Texas Rio Grande Valley, dumitru.caruntu@utrgv.edu

Christian A. Reyes
The University of Texas Rio Grande Valley

Recommended Citation

Caruntu, Dumitru I., and Christian A. Reyes. "Casimir Effect on Amplitude-Frequency Response of Parametric Resonance of Electrostatically Actuated NEMS Cantilever Resonators." Developments and Novel Approaches in Biomechanics and Metamaterials. Springer, Cham, 2020. 267-289. https://doi.org/10.1007/978-3-030-50464-9_15

Chapter 15
Casimir Effect on Amplitude-Frequency Response of Parametric Resonance of Electrostatically Actuated NEMS Cantilever Resonators

Dumitru I. Caruntu & Christian A. Reyes

Abstract This paper deals with the effect of Casimir force on the amplitude-frequency response of parametric resonance of electrostatically actuated nano-resonators. The resonator is actuated by using an electrostatic force to include a first order fringe correction. Casimir force and viscous damping force are included in the model, as well. Both electrostatic and Casimir forces are nonlinear. The behavior of the resonator is investigated using two methods, the Method of Multiple Scales (MMS) for a Reduced Order Model (ROM) using one mode of vibration, and numerical integration of ROMs using up to five modes of vibration. ROM is based on the application of a Galerkin procedure that uses the undamped mode shapes of the cantilevered beam as the basis of functions. The amplitude-frequency response consists of two bifurcations, namely subcritical and supercritical. The increase of Casimir effect shows an increase of the interval of frequencies of the unstable zero steady-state solutions, and a larger range of frequencies for which the system has stable steady-state solutions for amplitudes larger than 0.5 of the gap.

Keywords: NEMS · Non-linear · Amplitude-frequency · Parametric resonance · Casimir effect

15.1 Introduction

Nano-electromechanical systems (NEMS) are of great interest in the development of miniaturized sensors (Zhang and Turner, 2005; Zhu et al, 2007; Caruntu et al, 2019; Cheng et al, 2007; Cimalla et al, 2007; Zhang et al, 2014), filters (Rhoads et al, 2005; Lamoreaux, 2004), resonators (Caruntu and Oyervides, 2017; Nayfeh

D. I. Caruntu, C. A. Reyes
University of Texas Rio Grande Valley,
Mechanical Engineering Department, Edinburg, Texas 78539, U.S.A.
e-mail: caruntud2@asme.org, c.reyes47@gmail.com

et al, 2007; Nayfeh and Younis, 2005; Caruntu and Juarez, 2019; Younis and Nayfeh, 2003; Alsaleem et al, 2009; Zhu et al, 2007; Ke, 2009; Blom et al, 1992; Caruntu and Knecht, 2011, 2015; Caruntu and Taylor, 2014), actuators (Zand and Ahmadian, 2009; Hu et al, 2004; Younis et al, 2003; Daqaq et al, 2009; Batra et al, 2006; Krylov, 2008; Caruntu et al, 2013b), and switches, motors and relays (Lamoreaux, 2004). NEMS have numerous applications due to their low power consumption, ease of fabrication, high efficiency, simple structure, and quick response. These applications can be achieved via a variety of element configurations and actuation methods (Zhang et al, 2014). Electrostatic actuation could be used for such NEMS configurations (Caruntu and Knecht, 2011). One of the critical effects in electrostatically actuated devices is the presence of pull-in instability which arises due to nonlinearities in the system. Pull-in occurs when a moving element contacts and "sticks" to another element within the system. In many systems, this is a major limitation as it can significantly limit the range of motion of the device (Zhang et al, 2014; Caruntu et al, 2016). Hence, it is of great interest to predict how system parameters influence pull-in in order to control or mitigate its effects.

Nonlinearities can arise from a number of sources such as geometric nonlinearities due to large deflections (Spagnuolo and Andreaus, 2019; Baroudi et al, 2019), squeeze-film damping effects, and actuating forces. In particular, capacitive electrostatic forces are commonly used as the actuating force in nano devices and introduce nonlinear effects. Additionally, at submicron scales, intermolecular surface forces, such as Casimir or van der Waals, can affect the behavior of micro- and nano-beams as well (Ramezani et al, 2007; Caruntu and Juarez, 2019).

The Casimir force and a first order fringe effect models that are considered here are reported by Ramezani et al (2008). The electrostatic excitation produced by a fluctuating voltage across the length of the nano-beam parametrically excites the system. Specifically, a parametric term arises in both linear and nonlinear terms of the equation of motion. This is similar to Rhoads et al (2006) who investigated a parametrically excited comb drive system. It was found that such an excitation does not create just a single defined type of nonlinear effect for the system, but a variety of effects depending on system parameters in addition to the frequency and amplitude of excitation. Various bifurcations were found in the system in which the frequency of excitation was used as the bifurcation parameter. These bifurcations created mixed nonlinearities in addition to the familiar hardening and/or softening effects. In this paper, a parametrically excited cantilevered nano-beam is investigated and similar frequency dependant bifurcations are found.

Understanding the effect of parametric excitations is of general interest. The stability of these systems and the types of nonlinearities that occur are highly sensitive to physical parameters as well as frequency and initial amplitude (Nayfeh et al, 2007; Nayfeh and Younis, 2005; Younis and Nayfeh, 2003; Alsaleem et al, 2009; Rhoads et al, 2006; Caruntu et al, 2016). It is then important to identify bifurcation parameters and bifurcation points in order to design and control systems under parametric excitation. Bifurcation phenomena have been investigated in literature for such parametrically excited systems, mainly for discrete comb drive systems (Rhoads et al, 2006; DeMartini et al, 2007), but not for cantilevered beam elements. Most of

the analysis in literature investigated pull-in stability, amplitude-frequency responses or found limit cycles and time responses of such systems (Zand and Ahmadian, 2009; Ramezani et al, 2008). Daqaq et al (2009) discussed how parametric excitations in a cantilevered beam coupled to an electrical system via a piezoelectric patch can be used for energy harvesting. They found that there is an optimal value for the electromechanical coupling terms for maximizing the output voltage of the harvester. They also discussed the sensitivity for the harvester in that there is a critical value for excitation forces below which oscillations will not occur. The value of the critical excitation force is dependent on the electromechanical coupling term.

Ke (2009) investigated a double-sided electromechanically driven nanotube resonator taking into account van der Waals forces. An energy based method was used to find analytical relationships for the steady state amplitude of the nanotube as a function of driving frequency and excitation voltage. An analytical relationship for the resonant pull-in voltage was also developed. The analytical results where then verified numerically using a reduced order Galerkin method carried out to 5th order. Sedighi et al (2014) investigated electrostatically actuated nano cantilever including the Casmir and van der Waals force using the Parameter Expansion Method.

In this paper, an investigation of the effect of the Casimir forces on the amplitude-frequency response of parametric resonance of electrostatically actuated NEMS cantilever resonators is conducted. Forces acting on the resonator are 1) electrostatic forces to include fringe effect, given by an AC voltage of frequency near natural frequency of the cantilever, 2) Casimir force due to the gap between the resonator and a parallel ground plate less than 1μm, and 3) viscous damping force. All forces are in the category of soft excitation, and weak nonlinearities and damping. In the case of soft excitation the structure experiences very small amplitudes if not in a resonant zone.

To the best of our knowledge, this is the first time when 1) the Casimir forces effect on the amplitude-frequency response is investigated using 2) ROMs up to five modes of vibration. 3) ROM with one mode of vibration, and all nonlinear terms expanded in Taylor series with all terms up to cubic power retained is solved using the Method of Multiple Scales (MMS). 4) ROMs with two, three, four, and five modes of vibration are numerically integrated using a MATLAB ode solver, namely ode15s, in order to predict time response of the resonator. 5) ROMs with up to five modes of vibration are used to perform a continuation and bifurcation analysis using AUTO 07p software package. 6) This work shows that ROM with five modes of vibration accurately predict the amplitude-frequency bifurcation diagram (response) in all amplitudes up to the gap. 7) Casimir forces effect on the amplitude-frequency response shows that as Casimir forces increase, the softening effect increases and the bifurcation points (as well as the entire steady-state amplitudes) are shifted to lower frequencies.

15.2 System Model

In the present model of the NEMS cantilever resonator, the Euler–Bernoulli theory of thin beams is used. The resonator is a uniform cantilever.

Electrostatic force is a common source of actuation in Nano-electromechanical system (NEMS) devices. On micro- and nano-scales, electrostatic actuation is able to provide sizable forces with relatively low voltages and power consumption. The Palmer approximate formula (a first order fringing correction) gives the electrostatic force per unit length as follows:

$$F_e = \frac{\varepsilon_0 W}{2} \frac{V(t)^2}{(g-w)^2} \Big[1 + 0.65 \frac{(g-w)}{W}\Big] \tag{15.1}$$

where ε_0 is the permittivity of free space, W is the beam width, g is the gap between the beam and the ground plate, w is the deflection of the beam, and $V(t)$ is the applied voltage.

Between the beam and the ground plate is a dielectric material such as air. The actuation forces are given by the Casimir effect and electrostatic force produced by a potential difference across the upper beam and underlying ground conducting plate.

The Casimir force is significant for nano-scale systems, and it accounts for the dispersion forces which arise between closely spaced, uncharged conducting surfaces. In the context of the system used in this paper, plate separations are large enough when pair interactions between atoms and molecules (referred to as the van der Waals interaction following a $1/d^3$ relation) are considered non-significant, and the force between plates depends on only bulk material properties (this is sometimes referred to as the retarded van der Waals interaction following a $1/d^4$ relation). This occurs when the separation of surfaces is significantly larger than the atomic spacing. The transition between the van der Waals and Casimir regime occurs at a distance of approximately 20 nm (Ramezani et al, 2008) and hence a larger gap distance will be considered in this investigation. On the other hand, in order for the Casimir effect to be significant, surface separations should be less than approximately 1000 nm. The Casimir force per unit length along the beam is (Lamoreaux, 2004)

$$F_c = \frac{\pi^2 \hbar c W}{240(g-w)^4} \tag{15.2}$$

where $\hbar = 1.055 \times 10^{-34}$ Js is Planck's constant divided by 2π, and $c = 2.998 \times 10^8\ \mathrm{ms}^{-1}$ is the speed of light. The source of this effect is a matter of debate but is typically attributed to a zero-point energy in the electromagnetic field. Casimir's original derivation of Eq. (15.2) is based on this assertion, and with the experimental verification of this effect has been argued as proof of zero-point energy. Other approaches, however, have been used to explain the Casimir force completely removed from zero-point energy resulting in the identical results of Eq. (15.2). One of these alternative approaches was proposed by Lifshitz who attributed the phenomena to charge and current fluctuations due to Johnson noise. These fluctuations within a

material produce a field that can extend beyond its surface resulting in an attractive force at very small distances (Lamoreaux, 2004).

When modeling structures at the micro and nano scale, air damping effects are significant and impact the behavior of the system. Viscous flow as the beam moves through the air is one of the main components of air damping. The force due to viscous damping is described by

$$F_d = b\frac{\partial w}{\partial t} \tag{15.3}$$

where b is the coefficient of viscous damping per unit length.

15.3 Partial-Differential Equation of Motion

The flexible silicon nano cantilever resonator suspended over a grounded substrate (underlying plate), Fig. 15.1, is electrostatically actuated by applying a potential difference between the cantilever and the ground plate. In addition to the electrostatic force, Casimir and viscous damping forces are included in the model. The length of the beam is considered to be relatively long compared to the underlying gap and hence the beam will experience only small to moderate deflections, i.e. the slope of the beam will be relatively small, so the Euler–Bernoulli theory is suitable. This is important since the model used to describe the electrostatic and Casimir forces assumes the upper and lower plates to be locally parallel.

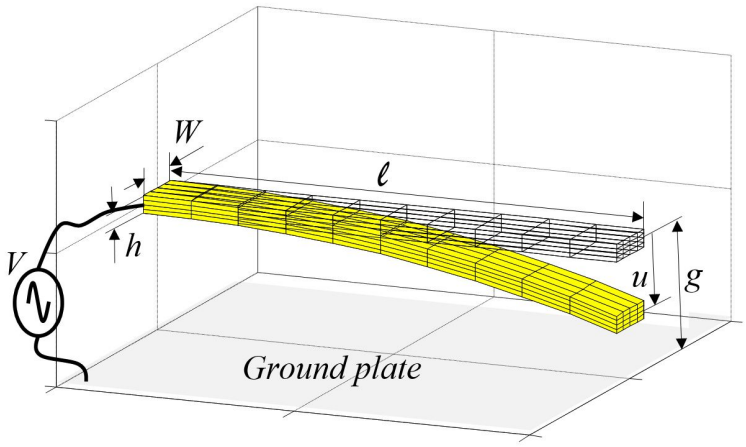

Fig. 15.1 Electrostatically Actuated Uniform NEMS Resonator

The dimensionless equation of motion of the resonator (Caruntu and Knecht, 2011; Caruntu and Martinez, 2014) to include boundary and initial conditions, is given by

$$\begin{cases} \dfrac{\partial^4 u(\tau,z)}{\partial z^4}+\dfrac{\partial^2 u(\tau,z)}{\partial \tau^2}= -b^*\dfrac{\partial u(\tau,z)}{\partial \tau}+\dfrac{\alpha}{[1-u(\tau,z)]^4}+ \\ \qquad\qquad \dfrac{\delta V^2}{[1-u(\tau,z)]^2}+\dfrac{f\delta V^2}{1-u(\tau,z)} \\ u(\tau,0)=\dfrac{\partial u}{\partial z}(\tau,0)=\dfrac{\partial^2 u}{\partial z^2}(\tau,1)=\dfrac{\partial^3 u}{\partial z^3}(\tau,1)=0 \\ u(0,z)=f(z),\dfrac{\partial u}{\partial z}(0,z)=p(z) \end{cases} \tag{15.4}$$

One can see at the right-hand side of the differential equation of motion the dimensionless forces acting on the cantilever; from left to right, they are damping, Casimir, electrostatic, and fringe effect forces. Variables z, τ and $u(\tau,z)$ are dimensionless longitudinal coordinate, dimensionless time, and dimensionless deflection, respectively, and they are related to their corresponding dimensional quantities x, t, and $w(t,x)$, respectively, as follows:

$$u=\ w/g\ ,\quad z=x/\ell\ ,\quad \tau=t\cdot\frac{1}{\ell^2}\sqrt{\frac{EI_0}{\rho A_0}}\ , \tag{15.5}$$

where ℓ , g, E, A_0, I_0, and ρ are the beam's length, initial gap between cantilever and ground plate, Young's modulus, cross section area, cross section moment of inertia, and material density, respectively. The dimensionless parameters $\alpha,\ \delta,\ f$ and b^* in Eqs. (15.4) track the effects of Casimir forces, voltage (or electrostatic excitation amplitude), fringe, and damping, respectively, and they are given by

$$\alpha=\frac{\pi^2\hbar c W\ell^4}{240g^5EI_0},\ \delta=\frac{\varepsilon_0 W\ell^4}{2g^3EI_0}V_0^2,\ f=\frac{0.65g}{W},\ b^*=b\frac{\ell^2}{\sqrt{\rho A_0 EI_0}} \tag{15.6}$$

where b is the dimensional damping, and V_0 the voltage amplitude. In this investigation, the dimensionless voltage $V(\tau)$, dimensionless frequency of excitation Ω, and the dimensionless natural frequency ω are as follows:

$$V(\tau)=\cos\big(\Omega\tau\big),\quad \Omega=\Omega^*\ell^2\sqrt{\frac{\rho A_0}{EI_0}},\quad \omega=\omega^*\ell^2\sqrt{\frac{\rho A_0}{EI_0}} \tag{15.7}$$

where Ω^* is the dimensional frequency of excitation, and ω^* is the dimensional natural frequency of the resonator. The quality factor is related to dimensionless damping (Caruntu and Knecht, 2011).

15.4 Method of Multiple Scales

In what follows, the case of weak nonlinear forces and damping is considered, i.e. the Casimir, electrostatic, fringe, and damping parameters $\alpha,\ \delta,\ f$, and b^* in Eq. (15.4) are small. The Casimir, electrostatic, and fringe effect terms in Eq. (15.4) are expanded in Taylor series around $u = 0$ and all terms up to cubic power are retained. Then MMS is applied. A small dimensionless bookkeeping parameter ε is introduced as factor of all small terms in the resulting equation

$$\frac{\partial^2 u}{\partial \tau^2} + \frac{\partial^4 u}{\partial z^4} = -\varepsilon b^* \frac{\partial u}{\partial \tau} + \varepsilon\alpha\big[1 + 4u + 10u^2 + 20u^3\big] + \varepsilon\delta\big[\big(1+f\big) + \big(2+f\big)u + \big(3+f\big)u^2 + \big(4+f\big)u^3\big]V^2(\tau) \quad (15.8)$$

A first-order expansion of the dimensionless transverse displacement u is considered. This is given by

$$u(z,\tau,\varepsilon) = u_0(z,T_0,T_1) + \varepsilon \cdot u_1(z,T_0,T_1) \quad (15.9)$$

where $T_0 = \tau$ is fast time scale and $T_1 = \varepsilon \cdot \tau$ is slow time scale. The time derivatives become

$$\partial/\partial\tau = D_0 + \varepsilon \cdot D_1,\ D_n = \partial/\partial T_n,\ n = 0,1 \quad (15.10)$$

where $D_n,\ n = 0,1$ represent partial derivatives with respect to the fast and slow time scales. Substituting Eq. (15.9) and Eq. (15.10) into Eq. (15.8), and equating coefficients of like powers of the bookkeeping parameter, the following two approximation problems, namely zero-order and first-order, result

$$\text{Order } \varepsilon^0 : D_0^2 u_0 + \frac{\partial^4 u_0}{\partial z^4} = 0 \quad (15.11)$$

$$\text{Order } \varepsilon^1 : D_0^2 u_1 + \frac{\partial^4 u_1}{\partial z^4} = -2D_0 D_1 u_0 - b^* D_0 u_0 + \alpha\big[1 + 4u_0 + 10u_0^2 + 20u_0^3\big] + \delta\big[\big(1+f\big) + \big(2+f\big)u_0 + \big(3+f\big)u_0^2 + \big(4+f\big)u_0^3\big]V^2\big(T_0\big) \quad (15.12)$$

The solution u_0 of Eq. (15.11) is given by

$$u_0\big(z,T_0,T_1\big) = \varphi(z)\big[A\big(T_1\big)e^{i\omega T_0} + \overline{A}\big(T_1\big)e^{-i\omega T_0}\big] \quad (15.13)$$

where A and $\overline{A}$ are complex conjugate coefficients depending on the slow time scale. Enforcing the boundary conditions given by Eq. (15.4), the mode shapes $\varphi_k\big(z\big)$ and the corresponding natural frequency ω_k are obtained. Natural frequencies and mode shapes for uniform cantilevers are reported in the literature Alsaleem et al (2009) and Zhu et al (2007); Caruntu and Knecht (2011). Natural frequencies and mode shapes of nonuniform structures as well as mathematical methods for finding them can be found in the literature Caruntu (2007, 2005, 2013). The mode shapes $\varphi_k\big(z\big)$ of a uniform cantilever form an orthonormal set, satisfying

$$\langle \varphi_k(z), \varphi_n(z) \rangle = \int_0^1 \varphi_k(z)\varphi_n(z)dz = \delta_{kn} \ , \ \frac{d^4\varphi_k(z)}{dz^4} = \omega_k^2 \varphi_k(z) \\ \varphi_k(0) = 0, \ \varphi_k'(0) = 0, \ \varphi_k''(1) = 0, \ \varphi_k'''(1) = 0 \ . \tag{15.14}$$

where δ_{kn} is Kronecker's delta. The first-order approximation can be found by solving the nonhomogeneous Eq. (15.12). Substituting Eq. (15.13) into Eq. (15.12) , it results

$$\begin{aligned} &D_0^2 u_1 + \frac{\partial^4 u_1}{\partial z^4} = -2D_0 D_1 \varphi_k \left[A_k(T_1)e^{i\omega_k T_0} + \overline{A_k}(T_1)e^{-i\omega_k T_0}\right] \\ &- b^* D_0 \varphi_k \left[A_k(T_1)e^{i\omega_k T_0} + \overline{A_k}(T_1)e^{-i\omega_k T_0}\right] + \alpha\Big\{1 + 4\varphi_k\left[A_k(T_1)e^{i\omega_k T_0}\right. \\ &\left. + \overline{A_k}(T_1)e^{-i\omega_k T_0}\right] + 10\varphi_k^2\left[A_k(T_1)e^{i\omega_k T_0} + \overline{A_k}(T_1)e^{-i\omega_k T_0}\right]^2 \\ &+ 20\varphi_k^3\left[A_k(T_1)e^{i\omega_k T_0} + \overline{A_k}(T_1)e^{-i\omega_k T_0}\right]^3\Big\} + \delta\Big\{(1+f) + \\ &(2+f)\varphi_k\left[A_k(T_1)e^{i\omega_k T_0} + \overline{A_k}(T_1)e^{-i\omega_k T_0}\right] + (3+f)\varphi_k^2\left[A_k(T_1)e^{i\omega_k T_0} + \right. \\ &\left.\overline{A_k}(T_1)e^{-i\omega_k T_0}\right]^2 + (4+f)\varphi_k^3\left[A_k(T_1)e^{i\omega_k T_0} + \overline{A_k}(T_1)e^{-i\omega_k T_0}\right]^3\Big\}V^2(T_0)^2 \end{aligned} \tag{15.15}$$

In this investigation the AC frequency of excitation is considered near natural frequency $\Omega \approx \omega_k$. This nearness is showed by a small detuning parameter σ as follows:

$$\Omega = \omega_k + \varepsilon\sigma \tag{15.16}$$

Equation (15.15) is then expanded. The square of the dimensionless voltage V is given by

$$V^2(T_0) = \frac{1}{2} + \frac{1}{4}\left(e^{2i\Omega T_0} + e^{-2i\Omega T_0}\right) \tag{15.17}$$

After substituting Eq. (15.16) and Eq. (15.17) into Eq. (15.15), the secular terms containing $\left(e^{i\omega_k T_0}\right)$ are collected and their sum set equal to zero. In addition, the non-homogeneous Eq. (15.15) has to be orthogonal to every solution of the homogeneous problem Eq. (15.11), so the equation of secular terms becomes

$$\begin{aligned} &-2i\omega_k g_{1kk}A_k' - i\omega_k b^* g_{1kk}A_k + \left[4\alpha + C_2\right]g_{1kk}A_k + 3\left[20\alpha + C_4\right]g_{3kk}A_k^2\overline{A_k} + \\ &\frac{1}{2}C_2 g_{1kk}\overline{A_k}e^{2i\sigma T_1} + \frac{3}{2}C_4 g_{3kk}A_k\overline{A_k}^2 e^{2i\sigma T_1} + \frac{1}{2}C_4 g_{3kk}A_k^3 e^{-2i\sigma T_1} = 0 \end{aligned} \tag{15.18}$$

where

$$C_m = \frac{1}{2}(m+f)\delta, \qquad m = 1,2,3,4\,, \qquad g_{nkk} = \langle \varphi_k^n, \varphi_k \rangle = \int_0^1 \varphi_k^n \varphi_k dz \tag{15.19}$$

and n is greater than or equal to zero. A_k' is the derivative of A_k with respect to the slow time scale T_1. Express A_k in polar form

$$A_k = \frac{1}{2}a_k e^{i\beta_k} \tag{15.20}$$

where a_k and β_k are real and represent the amplitude of the beam and the phase of the system relative to the excitation frequency, respectively. Substituting Eq. (15.20) into Eq. (15.18) and separating the real and imaginary parts, the following amplitude-phase system of equations results

$$a_k' = a_k\left[-\frac{b^*}{2}+\left(C_2+\frac{C_4}{2}\frac{g_{3kk}}{g_{1kk}}a_k^2\right)\frac{\sin 2\gamma_k}{4\omega_k}\right] \tag{15.21}$$

$$a_k\gamma_k' = a_k\sigma+\frac{4\alpha+C_2}{2\omega_k}a_k+\frac{3\left(20\alpha+C_4\right)}{8\omega_k}\frac{g_{3kk}}{g_{1kk}}a_k^3 + a_k\left(C_2+C_4\frac{g_{3kk}}{g_{1kk}}a_k^2\right)\frac{\cos 2\gamma_k}{4\omega_k} \tag{15.22}$$

where

$$\gamma_k = \sigma T_1-\beta_k \tag{15.23}$$

The steady-state solutions result by substituting $a_k' = \gamma_k' = 0$ into Eqs. (15.21) and (15.22). One of the steady-state solutions is the trivial solution $a_k = 0$ for all values of the detuning parameter σ. The non-trivial steady state solution case consists of a set of parametric equations describing the amplitude-frequency bifurcation diagram (response) as follows:

$$a_k^2 = \frac{2g_{1kk}}{C_4 g_{3kk}}\left(\frac{2\omega_k b^*}{\sin 2\gamma_k}-C_2\right) \tag{15.24}$$

$$\sigma = -\frac{4\alpha+C_2}{2\omega_k}-\frac{3\left(20\alpha+C_4\right)}{8\omega_k}\frac{g_{3kk}}{g_{1kk}}\alpha_k^2-\left(C_2+C_4\frac{g_{3kk}}{g_{1kk}}a_k^2\right)\frac{\cos 2\gamma_k}{4\omega_k} \tag{15.25}$$

The MMS steady-state amplitudes of the amplitude-frequency response, Eqs. (15.24) and (15.25), are afterwards presented in Fig. 15.2 for a uniform beam. It is seen that a softening type of behavior occurs with two branches, lower and upper, which are unstable and stable, respectively.

15.5 Reduced Order Model of Uniform NEMS Cantilevers

The analytical results based on steady-state amplitudes which were obtained using MMS are compared to numerical solutions of Eq. (15.4), in the case of uniform resonators. The system is considered at nano scale, where the Casimir force is significant.

To numerically investigate the system, a reduced order model (ROM) is constructed (Alsaleem et al, 2009; Younis et al, 2003; Caruntu et al, 2013a). This is done by utilizing a Galerkin procedure in which the solution is

$$u(z,\tau)=\sum_{i=1}^{N}u_i(\tau)\varphi_i(z) \tag{15.26}$$

where $u_i(\tau)$ are time dependent functions to be determined, N the number modes of vibrations used, and $\varphi_i(z)$ the mode shape functions of the uniform cantilever. The mode shapes satisfy Eqs. (15.14).

It is important to note that when constructing ROM, the treatment of the excitation force is very important. It was reported by Younis et al (2003) that the exact form of the forcing function must be used to numerically solve the equations of motion accurately. It was shown that when the forcing function was Taylor expanded out to third order before solving, that erroneous results were predicted in amplitudes larger than 0.5 of the gap. In addition, for the solutions to converge, the number of terms in Eq. (15.26) must be at least $N=5$ (Caruntu et al, 2013b,c).

To implement the ROM, Eq. (15.4) is first multiplied by $(1-u)^4$ in order to eliminate any displacement terms from appearing in the denominator. Using Eq. (15.26) and (15.14), multiplying the resulting equation by $\varphi_n(z)$ and integrating from $z=0$ to 1, the following system of equations results

$$\begin{aligned}
&\sum_{i=1}^{N}\ddot{u}_i h_{ni}-4\sum_{ij=1}^{N}\ddot{u}_i u_j h_{nij}+6\sum_{ijk=1}^{N}\ddot{u}_i u_j u_k h_{nijk}-4\sum_{ijkl=1}^{N}\ddot{u}_i u_j u_k u_l h_{nijkl}\\
&+\sum_{ijklm=1}^{N}\ddot{u}_i u_j u_k u_l u_m h_{nijklm}+b^*\sum_{i=1}^{N}\dot{u}_i h_{ni}-4b^*\sum_{ij=1}^{N}\dot{u}_i u_j h_{nij}\\
&+6b^*\sum_{ijk=1}^{N}\dot{u}_i u_j u_k h_{nijk}-4b^*\sum_{ijkl=1}^{N}\dot{u}_i u_j u_k u_l h_{nijkl}\\
&+b^*\sum_{ijklm=1}^{N}\dot{u}_i u_j u_k u_l u_m h_{nijklm}+\sum_{i=1}^{N}\omega_i^2 u_i h_{ni}-4\sum_{ij=1}^{N}\omega_i^2 u_i u_j h_{nij}\\
&+6\sum_{ijk=1}^{N}\omega_i^2 u_i u_j u_k h_{nijk}-4\sum_{ijkl=1}^{N}\omega_i^2 u_i u_j u_k u_l h_{nijkl}\\
&+\sum_{ijklm=1}^{N}\omega_i^2 u_i u_j u_k u_l u_m h_{nijklm}=\delta V^2\Bigg[(1+f)\sum_{i=1}^{N}h_n\\
&-(2+3f)\sum_{i=1}^{N}u_i h_{ni}+(1+3f)\sum_{ij=1}^{N}u_i u_j h_{nij}+f\sum_{ijk=1}^{N}u_i u_j u_k h_{nijk}\Bigg]+\alpha h_n
\end{aligned} \tag{15.27}$$

where $n=1,2,\ldots,N$, and $i,j,k,l,m=1,2,\ldots,N$, and

$$h_n = \int_0^1 \varphi_n dz,\ h_{ni} = \int_0^1 \varphi_n \varphi_i dz,\ h_{nij} = \int_0^1 \varphi_n \varphi_i \varphi_j dz,$$
$$h_{nijk} = \int_0^1 \varphi_n \varphi_i \varphi_j \varphi_k dz,\ h_{nijkl} = \int_0^1 \varphi_n \varphi_i \varphi_j \varphi_k \varphi_l dz, \tag{15.28}$$
$$h_{nijklm} = \int_0^1 \varphi_n \varphi_i \varphi_j \varphi_k \varphi_l \varphi_m dz$$

Equations (15.27) form a system of N non-explicit coupled, nonlinear ordinary-differential equations. A finite number of terms N are used in Eq. (15.27). $N = 2, 3, 4,$ and 5 were the ROMs considered.

15.6 Numerical Simulations

The case of uniform cantilever beams is considered. The dimensionless cantilevers mode shapes, Eqs. (15.13) and (15.14) are reported by Weaver Jr et al (1990) and given by

$$\varphi_k(z) = -\Big\{\cos\big(\sqrt{\omega_k}z\big) - \cosh\big(\sqrt{\omega_k}z\big) + C_k\Big[\sin\big(\sqrt{\omega_k}z\big) - \sinh\big(\sqrt{\omega_k}z\big)\Big]\Big\} \tag{15.29}$$

where ω_k are the dimensionless natural frequencies. These frequencies and the constant coefficients C_k of the first five modes of vibration are given in Table 15.1 (Weaver Jr et al, 1990). Substituting Eq. (15.29) into Eq. (15.19) the coefficients g_{1kk}

Table 15.1 First five natural frequencies and mode shape coefficients for uniform cantilever

	$k=1$	$k=2$	$k=3$	$k=4$	$k=5$
ω_k	3.51602	22.0344	61.6972	120.9019	199.8595
C_k	-0.734	-1.0185	-0.9992	-1.00003	0.99999

and g_{3kk} can be obtained. The first mode $k = 1$ is considered. The g coefficients in this case are

$$g_{011} = 0.7830,\ g_{111} = 1.0000,\ g_{211} = 1.4778,\ g_{311} = 2.3488 \tag{15.30}$$

Similarly, substituting Eq. (15.29) into Eq. (15.28), the h coefficients of Eq. (15.27) are calculated. Table 15.2 gives the constants of the system. Table 15.3 shows values of physical characteristics of a typical nano-beam. This leads to realistic values of the dimensionless parameters given by Eqs. (15.6), and shown in Table 15.4. Substituting the values given in Table 15.4 and Eq. (15.30) into the steady-state Eqs. (15.24) and (15.25), the amplitude-frequency relationships are obtained.

Table 15.2 System Constants

Planck's constant/2π	$\hbar$	1.055×10^{-34} J s
Speed of light	c	2.998×10^{8} m/s
Permittivity of free space	ε_0	8.854×10^{-12} C^2/N/m^2

Table 15.3 Dimensional System Parameters

Beam width	W	125 nm
Beam length	l	132 μm
Beam thickness	h	165 nm
Initial gap distance	g	500 nm
Material density	ρ	2330 kg/m^3
Young's modulus	E	169 GPa
Quality factor	Q	350
Voltage	V_0	0.02 V

Table 15.4 Dimensionless System Parameters

Casimir parameter	α	0.01
Voltage parameter	δ	0.10
Fringe parameter	f	0.26
Damping parameter	b^*	0.01

Figure 15.2 shows the amplitude-frequency response using three different methods: MMS, 5T ROM AUTO, and 5T Time Response. In the horizontal axis is the detuning frequency σ, and in the vertical axis U_{max} the amplitude of the tip of the cantilever. MMS is a perturbation method used to solve a ROM with one mode of vibration and predict the amplitude-frequency response, Eqs. (15.24) and (15.25). 5TROM AUTO is a continuation and bifurcation analysis of ROM with five modes of vibration, Eqs. (15.27) with $N = 5$, by using the software package AUTO 07p in order to predict the amplitude-frequency response. 5T Time Response is a numerical integration of ROM with five modes of vibration, Eqs. (15.27) with $N = 5$, using ode15s, a MATLAB solver of ordinary differential equations, in order to obtain time responses of the structure. The three methods can be seen to be in good agreement at amplitudes lower than 0.4 of the gap. However, at higher amplitudes, MMS overestimates the amplitudes. At larger amplitudes 5T ROM AUTO and 5T Time responses are in good agreement.

The amplitude-frequency response consists of zero-amplitude steady-states, and two non-zero steady-state amplitude branches. The stable and unstable steady-state solutions are represented by solid and dashed lines, respectively. Nontrivial amplitudes resulting from Eqs. (15.24) and (15.25) are shown in Fig. 15.2. The solid

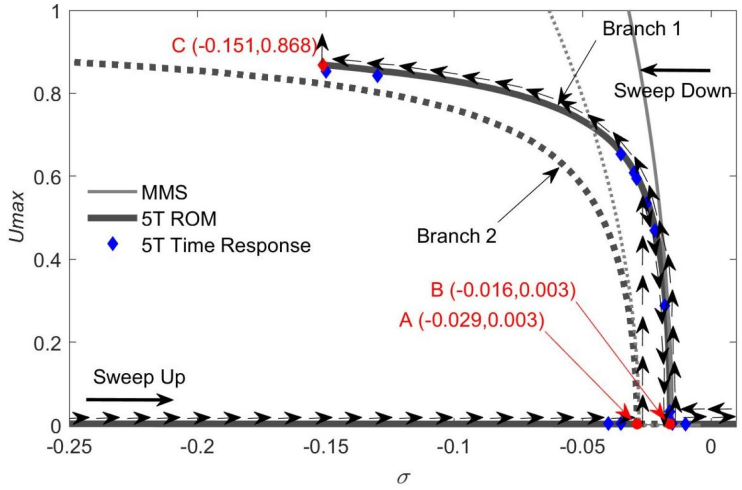

Fig. 15.2 Comparison between MMS, 5T ROM AUTO, and 5T Time Responses. $\alpha = 0.01$, $\delta = 0.1$, $b^* = 0.01$, and $f = 0.26$

branch 1, shows the stable steady-state amplitudes. The dashed branch 2, shows the unstable steady-state amplitudes. Zero amplitude solutions exist for all frequencies. The zero-amplitude solution is stable except for the detuning parameter values of $\sigma_A \leq \sigma \leq \sigma_B$. Two distinct bifurcations, one subcritical and the other one supercritical, are shown. Bifurcation points A and B are subcritical and supercritical bifurcation points, respectively. The results shown in Fig. 15.2 are similar to those reported by Rhoads et al (2006) for a parametrically excited comb drive. Zhu et al (2007) also obtained similar results in nonlinearly coupled micromechanical oscillators where a double pitchfork bifurcation was found with softening like characteristics. One can notice a softening nonlinear behavior of the system, i.e. the non-zero amplitude branches are bent towards lower frequencies. As the frequency is swept up, the system has zero steady-state amplitude until reaching the subcritical bifurcation point A. At this point the system loses stability and the system jumps to larger amplitudes located on branch 1. As the sweeping of frequency continues, the amplitude decreases along branch 1 until it reaches the supercritical bifurcation point B. After this point, the response continues with zero amplitudes. When the frequency is swept down, the system has zero steady-state amplitude until it reaches bifurcation point B. The amplitude starts increasing along branch 1 until it reaches the end of the branch, point C. After this point the system loses stability and pull-in occurs.

It should be noted that the results of Fig. 15.2 will never exceed unity since the beam displacement of the tip is being considered relative to the initial gap between the beam and ground electrode. If the beam's displacement does reach or approach unity it will experience a pull-in phenomenon. The only stable non-zero amplitudes

are found in a band around $-0.151 < \sigma < -0.016$. For frequencies to the right of the stable branch, $\sigma > -0.016$, all steady-state amplitudes are zero. For any given frequency to the left of the unstable branch, $\sigma < -0.029$, depending on the initial amplitude, the nano-cantilever settles either to zero steady-state amplitude, or larger steady-state amplitude on branch 1, or experiences pull-in.

Figure 15.3 shows the effect of the Casimir parameter on the amplitude-frequency response. As the Casimir force increases the response is shifted to lower frequencies. Both branches, along with the bifurcation points, are shifted as a whole. While the bifurcation points A and B are shifted to lower frequencies, the gap between them does not significantly change. However, the softening effect increases, i.e. the non-zero amplitude branches 1 and 2 are bent to a larger degree towards lower frequencies. Therefore the system starts experiencing lower amplitudes with greater Casimir parameter. The unstable branch experiences less bending from the influence of the Casimir force than the stable branch. This makes the stable branch get closer to the unstable branch, reducing the gap between both branches. The end point C of the stable branch 1 is shifted to lower frequencies as the Casimir force parameter increases.

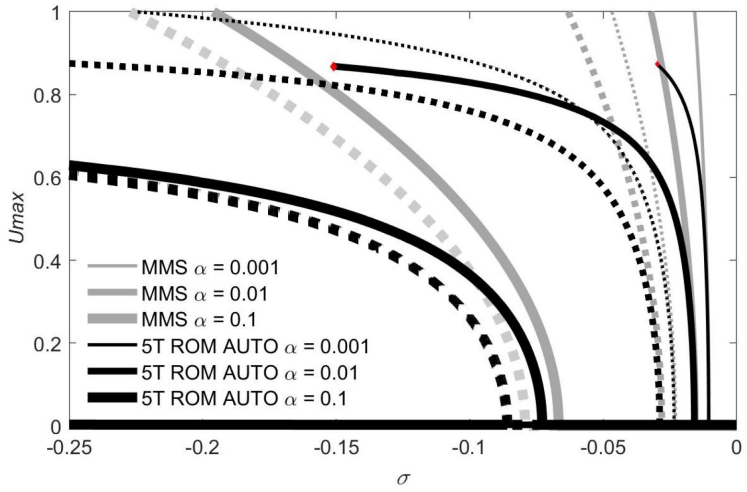

Fig. 15.3 Casimir influence on the frequency response using MMS and 5T ROM AUTO. $\delta = 0.1$, $b^* = 0.01$, and $f = 0.26$

Figures 15.4 through 15.6 show the time responses for specific frequencies and initial amplitudes. These time responses are in agreement with 5T ROM AUTO branches in Fig. 15.2. Time responses in Figures 15.4 and 15.5 settle to steady-state amplitudes on stable branches. For initial amplitudes below and above the unstable branch one can see that different steady-state amplitudes are reached for the same frequency, Figure 15.5 c) and d). Figure 15.6 shows two time responses in agreement

with the predicted last stable amplitude, point C, achieved at high amplitudes. A slight change in the frequency in Figure 15.6 shows that the nano-cantilever either settles to a steady-state amplitude on branch BC or experiences pull-in.

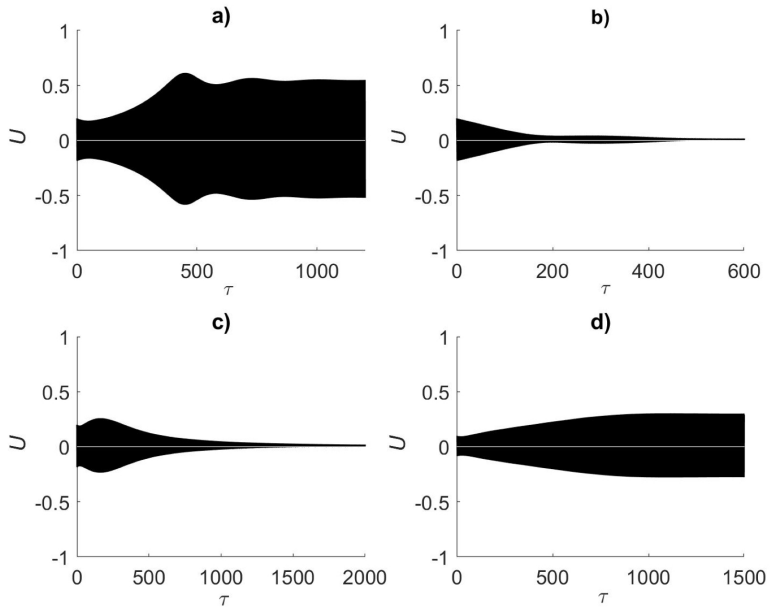

Fig. 15.4 Time Responses using five term (5T) ROM. $b^* = 0.01$, $f = 0.26$, $\delta = 0.1$, $\alpha = 0.01$ and a) $\sigma = -0.025$ with initial amplitude $U_0 = 0.2$, b) $\sigma = -0.035$ with initial amplitude $U_0 = 0.2$, c) $\sigma = -0.015$ with initial amplitude $U_0 = 0.2$, d) $\sigma = -0.018$ with initial amplitude $U_0 = 0.1$.

Figure 15.7 shows the convergence of the amplitude-frequency response when using MMS, 2 terms, 3 terms, 4 terms, and 5 terms ROM AUTO. When increasing the number of terms used in the ROM, the softening effect experienced in the system is better captured. The stable branch 1 with the end point C can be seen bending as the number of terms increases. For 4 and 5 term ROM AUTO the branches do not drastically change, so 5 term ROM AUTO is used in this research. The end point C of the stable branch can also be seen moving towards lower frequency as the number of terms increases. 5T ROM AUTO predicts the response and pull-in accurately.

Figure 15.8 and 15.9 show the convergence of the bifurcation points A and B with the number of terms of ROM. Both figures show that there is no significant difference between 4 and 5 term ROM AUTO, the responses overlapping each other.

Figure 15.10 shows the effect of the voltage parameter δ on the amplitude-frequency response of the resonator under Casimir force. One noticeable impact on the amplitude-frequency response is the frequency gap between the stable and unstable branches. As the voltage parameter increases, the frequency gap between

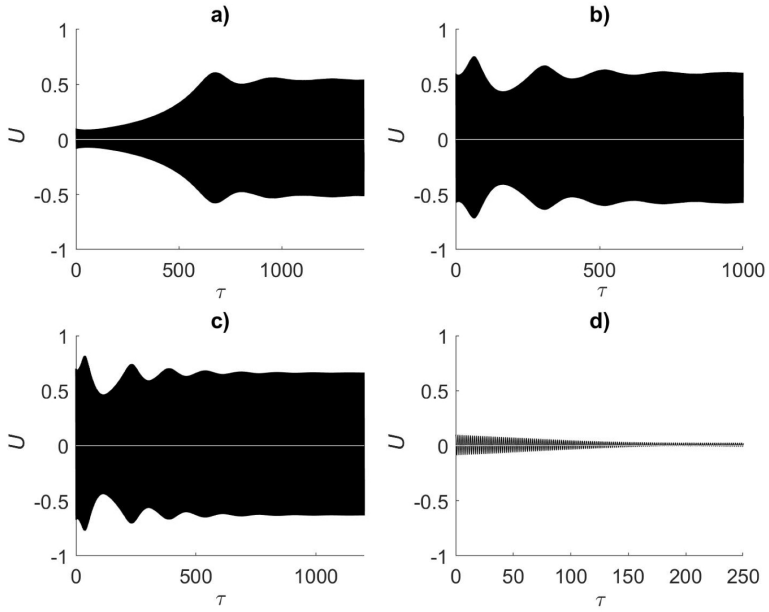

Fig. 15.5 Time Responses using five term (5T) ROM. $b^* = 0.01$, $f = 0.26$, $\delta = 0.1$, $\alpha = 0.01$ and a) $\sigma = -0.025$ with initial amplitude $U_0 = 0.1$, b) $\sigma = -0.029$ with initial amplitude $U_0 = 0.6$, c) $\sigma = -0.035$ with initial amplitude $U_0 = 0.7$, d) $\sigma = -0.035$ with initial amplitude $U_0 = 0.1$.

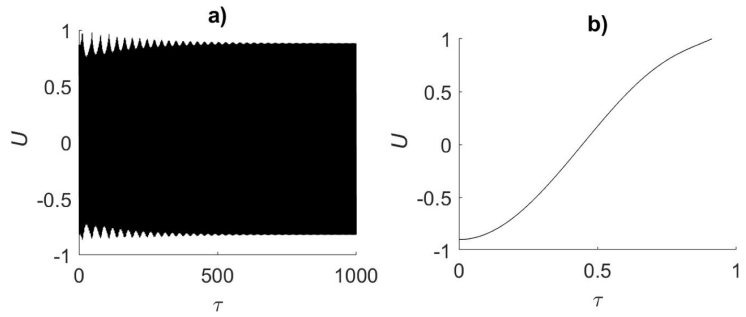

Fig. 15.6 Time Responses using five term (5T) ROM. $b^* = 0.01$, $f = 0.26$, $\delta = 0.1$, $\alpha = 0.01$ and a) $\sigma = -0.15$ with initial amplitude $U_0 = 0.87$, b) $\sigma = -0.16$ with initial amplitude $U_0 = 0.9$

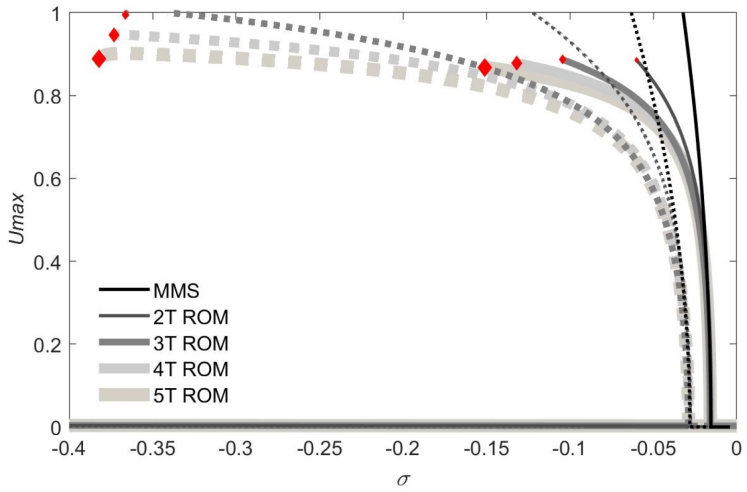

Fig. 15.7 Convergence of frequency response using MMS, 2 terms, 3 terms, 4 terms, and 5 terms ROM AUTO. $\alpha = 0.01$, $\delta = 0.1$, $b^* = 0.01$, and $f = 0.26$

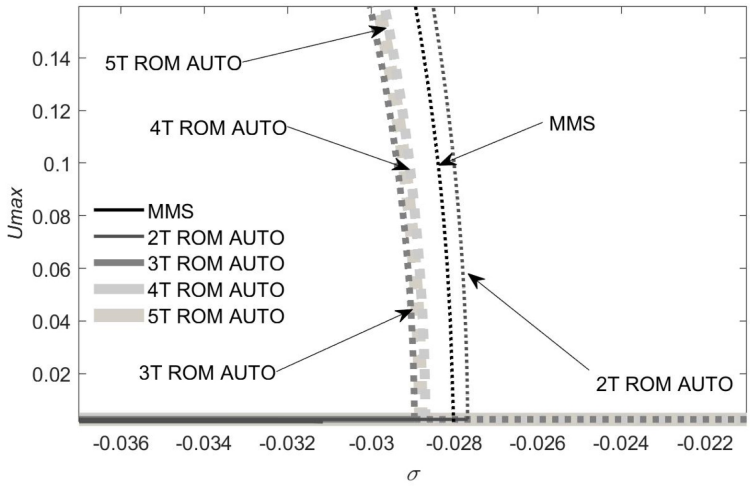

Fig. 15.8 Zoom in showing the convergence of the subcritical bifurcation point A with the number of terms in ROM.

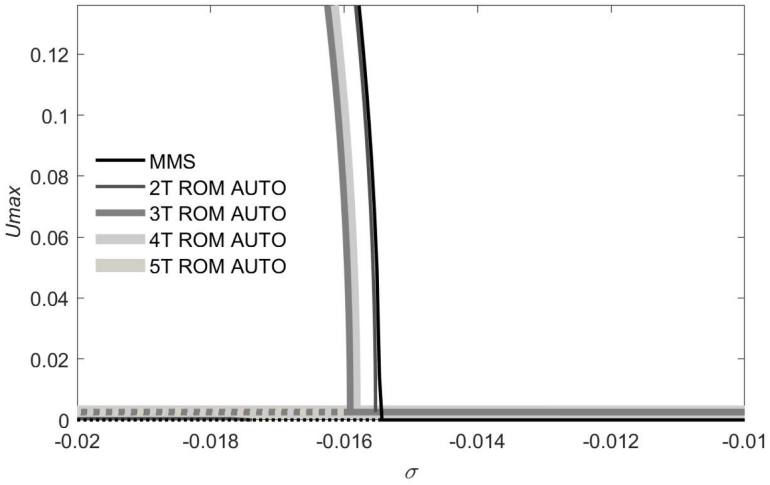

Fig. 15.9 Zoom in showing the convergence of the supercritical bifurcation point B with the numbers of terms in ROM.

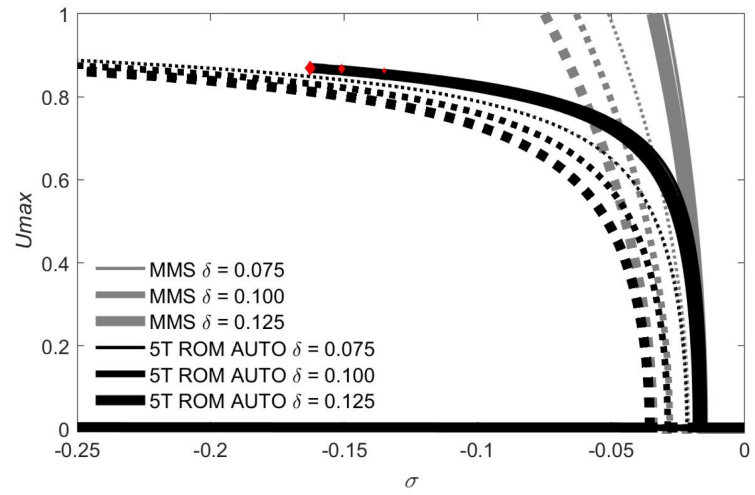

Fig. 15.10 Voltage influence on the frequency response using MMS and 5T ROM AUTO. $\alpha = 0.01$, $b^* = 0.01$, and $f = 0.26$

the stable and unstable branch increases due to shifting of the unstable branch, and the subcritical bifurcation point A, to lower frequencies. The stable branch and the supercritical bifurcation point B does not have a significant shifting. So, the zero-amplitude region between branches widens with an increase in the voltage parameter. Therefore, a larger voltage parameter δ increases the range of values of frequencies $\left(\sigma_A, \sigma_B\right)$ for which the resonator experiences non-zero steady-state amplitudes. The end point C of the stable branch is shifted to lower frequencies as the voltage parameter is increased. This causes the range of values of resonant frequencies $\left(\sigma_B, \sigma_C\right)$ for which the resonator can reach non-zero steady-state amplitudes to increase.

Figure 15.11 shows the effect of fringing parameter f on the amplitude-frequency response of the resonator under Casimir force. It is seen that as the fringe parameter increases, the stable and unstable branches are shifted to lower frequencies. Similar to the voltage effect, the unstable branch along with the subcritical bifurcation point A are significantly shifted towards lower frequencies with the increase of the fringe parameter. The supercritical bifurcation point B located on the stable branch is shifted towards lower frequencies as well, but the shifting is not significant. The end point C on the stable branch is shown to keep the same amplitude but is shifted towards lower frequencies. The unstable region $\left(\sigma_A, \sigma_B\right)$ between branches widens.

Since the value of the fringe effect parameter depends on gap to width ratio, resonators using narrow beam elements relative to the gap size should pay particular attention to the fringing that arises in the electrostatic field. The fringe effect enhances the electrostatic force.

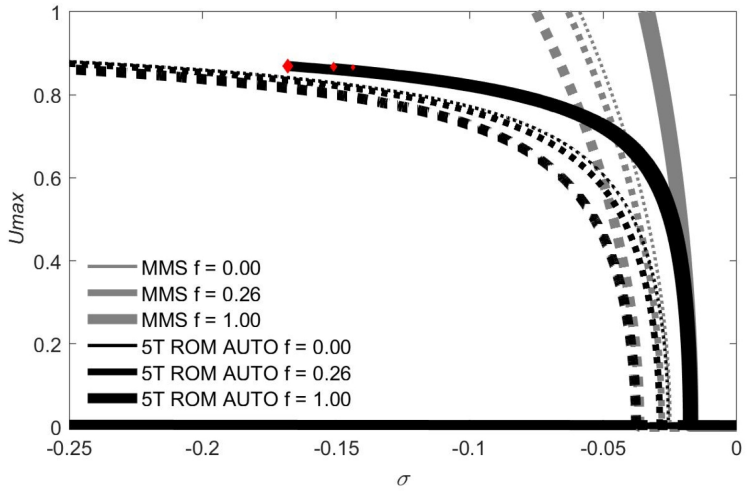

Fig. 15.11 Fringe effect on the frequency response using MMS and 5T ROM AUTO. $\alpha = 0.01$, $\delta = 0.1$, and $b^* = 0.01$

Figure 15.12 shows the effect of damping parameter on the amplitude-frequency response of the resonator under Casimir force. Increasing the damping parameter b^* the subcritical bifurcation point A is shifted to higher frequencies, while the supercritical bifurcation point B is shifted to lower frequencies. Therefore, as the damping is increased, the frequency gap between the stable and unstable branches, between points A and B as well, is reduced. At higher amplitudes, the end point C of the stable branch is shifted to higher frequencies. As for the unstable branch, there is minor change at higher amplitudes.

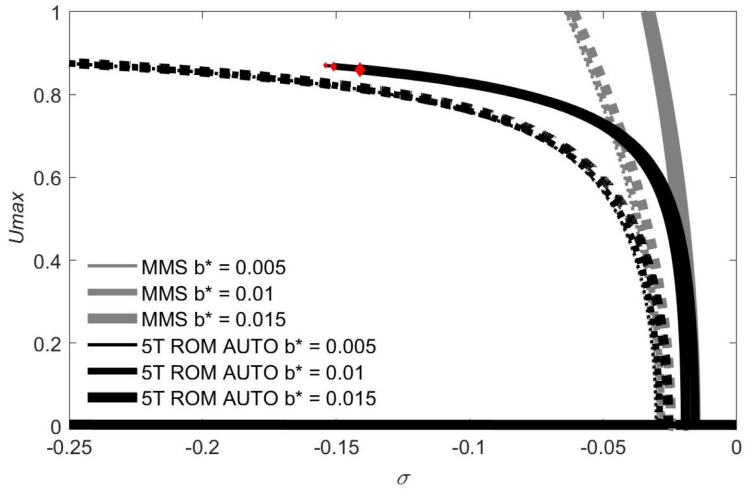

Fig. 15.12 Damping influence on frequency response using MMS and 5T ROM AUTO. $\alpha = 0.01$, $\delta = 0.1$, and $f = 0.26$

15.7 Discussion and Conclusions

This paper investigates the Casimir effect on the behavior of electrostatically actuated NEMS cantilever resonators under parametric resonance. Euler–Bernoulli beam theory was used for modeling the cantilevered beam under electrostatic actuation. AC voltage of frequency near natural frequency of the resonator was used to actuate the cantilever. This led the system into parametric resonance. The forces included in the model consisted of electrostatic force to include fringe effect, Casimir and damping forces. The effects of the dimensionless parameters on the amplitude-frequency response were investigated and reported.

After nondimensionalizing the equation of motion, two methods were used to solve the equation. The Method of Multiple Scales (MMS) was used in a direct

approach to find the amplitude-frequency relationship of the system. One should mention that MMS solved a ROM with one mode of vibration. The second method used was the Reduced Order Model method with up to five modes of vibration. ROM was based on a Galerkin procedure. ROM is accurate for strong nonlinearities. The amplitude-frequency responses from these two methods are compared. Although MMS captures the system's behavior quite well, it is limited to weak nonlinearities and small amplitudes. Nayfeh et al (2007); Nayfeh and Younis (2005) reported the use of ROM to predict periodic motions. Using ROM method with five modes of vibration, the response at higher amplitudes is better captured when compared to MMS. ROM captured also the behavior of the resonator for larger amplitudes including the pull-in instability. A similar ROM was used for the cantilevered resonator considered here using up to five modes of vibration. Using four or more modes guarantees the convergence of the steady state amplitude (Nayfeh et al, 2007; Younis et al, 2003). The results of the ROM where compared with the direct (Nayfeh et al, 2007) approach using the Method of Multiple Scales (MMS) for all cases.

It is important to note than both methods are in agreement for amplitudes less than 0.4 of the gap. The ROM is more accurate for amplitudes larger than 0.4 of the gap. However, the increased accuracy comes at a cost of increased computational time.

Acknowledgements We would like to acknowledge Martin W. Knecth and Roberto J. Zapata for their contributions to this work.

References

Alsaleem FM, Younis MI, Ouakad HM (2009) On the nonlinear resonances and dynamic pull-in of electrostatically actuated resonators. Journal of Micromechanics and Microengineering 19(4):045,013

Baroudi D, Giorgio I, Battista A, Turco E, Igumnov LA (2019) Nonlinear dynamics of uniformly loaded elastica: Experimental and numerical evidence of motion around curled stable equilibrium configurations. ZAMM-Zeitschrift für Angewandte Mathematik und Mechanik 99(7):1–20

Batra RC, Porfiri M, Spinello D (2006) Electromechanical model of electrically actuated narrow microbeams. Journal of Microelectromechanical systems 15(5):1175–1189

Blom F, Bouwstra S, Elwenspoek M, Fluitman J (1992) Dependence of the quality factor of micromachined silicon beam resonators on pressure and geometry. Journal of Vacuum Science & Technology B: Microelectronics and Nanometer Structures Processing, Measurement, and Phenomena 10(1):19–26

Caruntu D, Martinez I, Knecht M (2013a) Rom analysis of frequency response of AC near half natural frequency electrostatically actuated MEMS cantilevers. ASME J Comput Nonlinear Dyn 8(3):031,011

Caruntu DI (2005) Self-adjoint differential equations for classical orthogonal polynomials. Journal of Computational and Applied Mathematics 180(1):107–118

Caruntu DI (2007) Classical Jacobi polynomials, closed-form solutions for transverse vibrations. Journal of Sound and Vibration 306(3-5):467–494

Caruntu DI (2013) Factorization of self-adjoint ordinary differential equations. Applied Mathematics and Computation 219(14):7622–7631

Caruntu DI, Juarez E (2019) Voltage effect on amplitude–frequency response of parametric resonance of electrostatically actuated double-walled carbon nanotube resonators. Nonlinear Dynamics 98(4):3095–3112

Caruntu DI, Knecht M (2011) On nonlinear response near-half natural frequency of electrostatically actuated microresonators. International Journal of Structural Stability and Dynamics 11(04):641–672

Caruntu DI, Knecht MW (2015) Microelectromechanical systems cantilever resonators under soft alternating current voltage of frequency near natural frequency. Journal of Dynamic Systems, Measurement, and Control 137(4):041,016

Caruntu DI, Martinez I (2014) Reduced order model of parametric resonance of electrostatically actuated MEMS cantilever resonators. International Journal of Non-Linear Mechanics 66:28–32

Caruntu DI, Oyervides R (2017) Frequency response reduced order model of primary resonance of electrostatically actuated MEMS circular plate resonators. Communications in Nonlinear Science and Numerical Simulation 43:261–270

Caruntu DI, Taylor KN (2014) Bifurcation type change of AC electrostatically actuated MEMS resonators due to DC bias. Shock and Vibration 2014

Caruntu DI, Martinez I, Knecht MW (2013b) Reduced order model analysis of frequency response of alternating current near half natural frequency electrostatically actuated MEMS cantilevers. Journal of Computational and Nonlinear Dynamics 8(3):031,011

Caruntu DI, Martinez I, Taylor KN (2013c) Voltage–amplitude response of alternating current near half natural frequency electrostatically actuated MEMS resonators. Mechanics Research Communications 52:25–31

Caruntu DI, Martinez I, Knecht MW (2016) Parametric resonance voltage response of electrostatically actuated micro-electro-mechanical systems cantilever resonators. Journal of Sound and Vibration 362:203–213

Caruntu DI, Botello MA, Reyes CA, Beatriz JS (2019) Voltage–amplitude response of superharmonic resonance of second order of electrostatically actuated MEMS cantilever resonators. Journal of Computational and Nonlinear Dynamics 14(3):031,005

Cheng K, Weng Z, Oliver D, Thomson D, Bridges G (2007) Microelectromechanical resonator characterization using noncontact parametric electrostatic excitation and probing. Journal of Microelectromechanical Systems 16(5):1054–1060

Cimalla V, Niebelschütz F, Tonisch K, Foerster C, Brueckner K, Cimalla I, Friedrich T, Pezoldt J, Stephan R, Hein M, et al (2007) Nanoelectromechanical devices for sensing applications. Sensors and Actuators B: Chemical 126(1):24–34

Daqaq MF, Stabler C, Qaroush Y, Seuaciuc-Osório T (2009) Investigation of power harvesting via parametric excitations. Journal of Intelligent Material Systems and Structures 20(5):545–557

DeMartini BE, Butterfield HE, Moehlis J, Turner KL (2007) Chaos for a microelectromechanical oscillator governed by the nonlinear Mathieu equation. Journal of Microelectromechanical Systems 16(6):1314–1323

Hu YC, Chang C, Huang S (2004) Some design considerations on the electrostatically actuated microstructures. Sensors and Actuators A: Physical 112(1):155–161

Ke C (2009) Resonant pull-in of a double-sided driven nanotube-based electromechanical resonator. Journal of Applied Physics 105(2):024,301

Krylov S (2008) Parametric excitation and stabilization of electrostatically actuated microstructures. International Journal for Multiscale Computational Engineering 6(6):563–584

Lamoreaux SK (2004) The Casimir force: background, experiments, and applications. Reports on progress in Physics 68(1):201

Nayfeh AH, Younis MI (2005) Dynamics of MEMS resonators under superharmonic and subharmonic excitations. Journal of Micromechanics and Microengineering 15(10):1840

Nayfeh AH, Younis MI, Abdel-Rahman EM (2007) Dynamic pull-in phenomenon in MEMS resonators. Nonlinear dynamics 48(1-2):153–163

Ramezani A, Alasty A, Akbari J (2007) Closed-form solutions of the pull-in instability in nanocantilevers under electrostatic and intermolecular surface forces. International Journal of Solids and Structures 44(14-15):4925–4941

Ramezani A, Alasty A, Akbari J (2008) Analytical investigation and numerical verification of Casimir effect on electrostatic nano-cantilevers. Microsystem Technologies 14(2):145–157

Rhoads JF, Shaw SW, Turner KL, Baskaran R (2005) Tunable microelectromechanical filters that exploit parametric resonance. Journal of Vibration and Acoustics 127(5):423–430

Rhoads JF, Shaw SW, Turner KL, Moehlis J, DeMartini BE, Zhang W (2006) Generalized parametric resonance in electrostatically actuated microelectromechanical oscillators. Journal of Sound and Vibration 296(4-5):797–829

Sedighi HM, Daneshmand F, Zare J (2014) The influence of dispersion forces on the dynamic pull-in behavior of vibrating nano-cantilever based NEMS including fringing field effect. Archives of Civil and Mechanical Engineering 14(4):766–775

Spagnuolo M, Andreaus U (2019) A targeted review on large deformations of planar elastic beams: extensibility, distributed loads, buckling and post-buckling. Mathematics and Mechanics of Solids 24(1):258–280

Weaver Jr W, Timoshenko SP, Young DH (1990) Vibration problems in engineering. John Wiley & Sons

Younis MI, Nayfeh A (2003) A study of the nonlinear response of a resonant microbeam to an electric actuation. Nonlinear Dynamics 31(1):91–117

Younis MI, Abdel-Rahman EM, Nayfeh A (2003) A reduced-order model for electrically actuated microbeam-based MEMS. Journal of Microelectromechanical systems 12(5):672–680

Zand MM, Ahmadian M (2009) Vibrational analysis of electrostatically actuated microstructures considering nonlinear effects. Communications in Nonlinear Science and Numerical Simulation 14(4):1664–1678

Zhang W, Turner KL (2005) Application of parametric resonance amplification in a single-crystal silicon micro-oscillator based mass sensor. Sensors and Actuators A: Physical 122(1):23–30

Zhang WM, Yan H, Peng ZK, Meng G (2014) Electrostatic pull-in instability in MEMS/NEMS: A review. Sensors and Actuators A: Physical 214:187–218

Zhu J, Ru C, Mioduchowski A (2007) High-order subharmonic parametric resonance of nonlinearly coupled micromechanical oscillators. The European Physical Journal B 58(4):411–421